Ce 5*d* magnetic profile in Fe/Ce multilayers for the α and γ-like Ce phases by x-ray resonant magnetic scattering

N. Jaouen, J.M. Tonnerre, D. Raoux, E. Bontempi, and L. Ortega
Laboratoire de Cristallographie, CNRS, BP 16, 25 Avenue des Martyrs, 38042 Grenoble, France

M. Müenzenberg and W. Felsch
I. Physikalisches Institut Universität Göttingen, Bunsenstrasse 9, 37073 Göttingen, Germany

A. Rogalev
European Synchrotron Radiation Facility, 38043 Grenoble, France

H.A. Dürr, E. Dudzik, and G. van der Laan
Daresbury Laboratory, Daresbury, Warrington WA4 4AD, United Kingdom

H. Maruyama
Department of Physics, Faculty of Science, Okayama University, Okayama 700-8650, Japan

M. Suzuki
The Institute of Physical and Chemical Research (RIKEN), 323-3 Mihara, Mikazuki-cho, Sayo-gun, Hyogo 679-5413, Japan
(Received 18 February 2002; published 28 October 2002)

The in-depth distribution of the induced 5*d* magnetic moments across the Ce layers in Fe/Ce/La/Ce, Fe/La/Ce/La and Fe/$CeH_{2-\delta}$ multilayers has been investigated by x-ray resonant magnetic scattering (XRMS) at the Ce L_2 edge. The determination of the composition profile across the period of the multilayer is required for a quantitative analysis of XRMS and has been derived from x-ray resonant reflectivity measurements. In Fe/Ce/La/Ce and Fe/La/Ce/La multilayers, Ce adopts an α-like electronic configuration and the local magnetization, across the Ce layer, is found to be highly nonuniform. The Ce 5*d* magnetic profile shows an oscillating behavior with an amplitude decreasing from the Fe interface in Fe/Ce/La/Ce. Conversely, in Fe/La/Ce/La, where the Ce atoms are not in direct contact with Fe atoms, it presents an oscillatory profile with, however, a nearly constant amplitude. In Fe/$CeH_{2-\delta}$ multilayers, where hydrogen leads to a strain relaxation and to a 4*f* relocalization (Ce γ-like configuration), a nonoscillating decreasing profile has been observed. These experiments allow one to evidence an antiferromagnetic component in a α Ce ultrathin layer and a sharply decreasing induced magnetization due to 5*d*-3*d* hybridization at the interface.

DOI: 10.1103/PhysRevB.66.134420 PACS number(s): 75.70.−i, 71.27.+a, 71.28.+d, 78.70.Ck

I. INTRODUCTION

It is well established that magnetic multilayers exhibit a rich variety of novel effects related either to interface effects or to the confinement of electrons in ultrathin layers. These phenomena themselves depend on the growth process.[1–3] An important issue in the investigation of magnetic layer stacking is the influence of a spacer layer inserted in between two ferromagnetic layers. It has been shown that, depending on the thickness of the spacer layer, two ferromagnetic layers may be coupled parallel or antiparallel. Concomitant with that, the induced magnetism of the spacer layer has been evidenced.[4] It is of fundamental interest to determine the induced magnetization throughout a thin film in order to get better insight into the interactions between the ferromagnetic layer and the nonmagnetic one. It has been known for a long time that x-ray magnetic scattering provides direct information on the magnetic structure.[5] X-ray resonant magnetic scattering (XRMS) using either circularly[6–9] or linearly[10–12] polarized x rays, has proved to be a useful technique to study the magnetic properties of buried layer or interfaces and depth-dependent magnetic properties.

In the case of a magnetic multilayer, the periodicity of the magnetization leads to a magnetic contribution at the position of the low-angle Bragg peaks for ferromagnetic coupled multilayers[7,13,14] and in between the peaks for antiferromagnetic coupling.[7,15,16] Recently, we have shown that XRMS allows us to determine the spatial distribution of weak induced 5*d* magnetism through a Ce spacer layer in Fe/Ce multilayer.[4] The study of these one dimensional systems permits us to probe the depth dependent interaction between the 5*d* Ce electronic states and the 3*d* states of Fe,[17] which has fascinating consequences, such as, for instance, the unusual properties of the ferromagnet $CeFe_2$.[18] In the stacked Ce/Fe systems, for a thickness smaller than 25 Å, Ce adopts an α-like electronic configuration with a magnetic order[18] in contrast to the α phase of Ce metal which is nonmagnetic. While the magnetic ordering is relatively well understood for elemental rare earths, the 5*d* magnetization of Ce is much more complex because of its 4*f* electronic states which are at the borderline between localization and itinerancy. For the α-like phase in Ce/Fe multilayers, two different regimes for the distribution of magnetic moments throughout the Ce layers have been observed by measurements of x-ray magnetic

 ©2002 The American Physical Society

circular dichroism (XMCD) as a function of the Ce layer thickness.[19] In regime 1, the mean 5*d* magnetic polarization decreases sharply from the interface up to a distance of 10–12 Å. Beyond that thickness, in regime 2, it decreases slowly with the inverse of the Ce thickness. Surprisingly the 4*f* magnetic polarization does not adopt the same behavior and appears to be restricted in the immediate interface. This intriguing behavior suggests that within a few Å from the Fe interface, the Ce 5*d* states are polarized through hybridization with the spin-split 3*d* states of Fe, while in regime 2, the magnetic order on the 5*d* states would not result from such a mechanism but instead would be an intrinsic property of the ground state of α-like Ce itself in the multilayer.[19] Our previous XRMS experiment on [Ce/Fe] and [La/Fe] confirmed that the α-like Ce 5*d* polarization extends far from Fe interface but more surprisingly showed that the Ce layers exhibit an oscillating magnetic profile.[4] It corresponds to the sum of two damped oscillating profiles originating from the interfaces.

In this paper, we would like to focus on the interface effect which, through the contact between Fe and Ce atoms, favors a direct hybridization and therefore induces magnetism in Ce. On the one hand, we investigate the Ce 5*d* magnetic profile, in a [Fe/Ce(15 Å)/La(10 Å)/Ce(15 Å)] multilayer in order to probe the features of the oscillation in a 15-Å-thick layer, being in contact with the Fe only on one side. On the other hand, we investigate the Ce magnetic profile in a [Fe/La(15 Å)/Ce(10 Å)/La(15 Å)] multilayer where a 15-Å-thick La layer has been inserted at the interfaces to avoid a direct contact between the Ce and Fe layers. It has been shown that the 5*d* levels of La are magnetically polarized by the 3*d*-5*d* hybridization at interface.[4,17] However, the extension is limited to the two first atomic planes (5–6 Å). Although there is no magnetization of La at the La/Ce interfaces, XMCD measurements[20] have shown that, in this system, the Ce 5*d* states are still magnetized while no 4*f* polarization has been observed. This is an important difference compared with the first system which prompts us to understand how a magnetic order on the Ce 5*d* states can exist without a polarization of the 4*f* states. Since Ce or La have an atomic size quite different from that of Fe, a strain may occur at the interface and be also a source of structural change that can influence the magnetic properties. In order to investigate such an effect, we will discuss the Ce 5*d* mag-

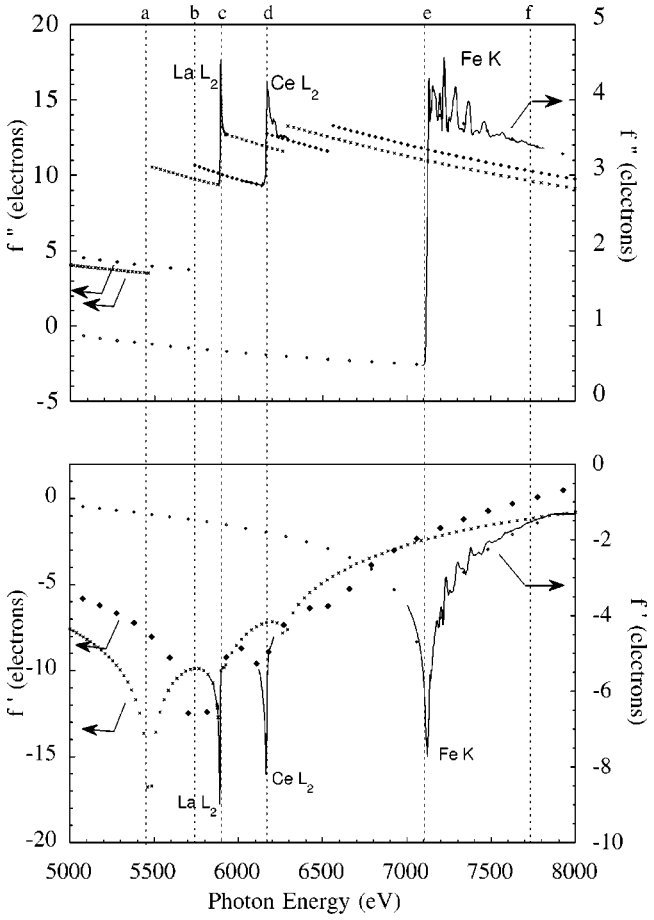

FIG. 1. Energy dependence of the imaginary and real corrections f'' and f', respectively, to the atomic scattering factor for La, Ce, and Fe. This lines show selected energies ($a=5475$ eV, $b=5715$ eV, $c=5887$ eV, $d=6160$ eV, $e=7107$ eV, $f=7705$ eV).

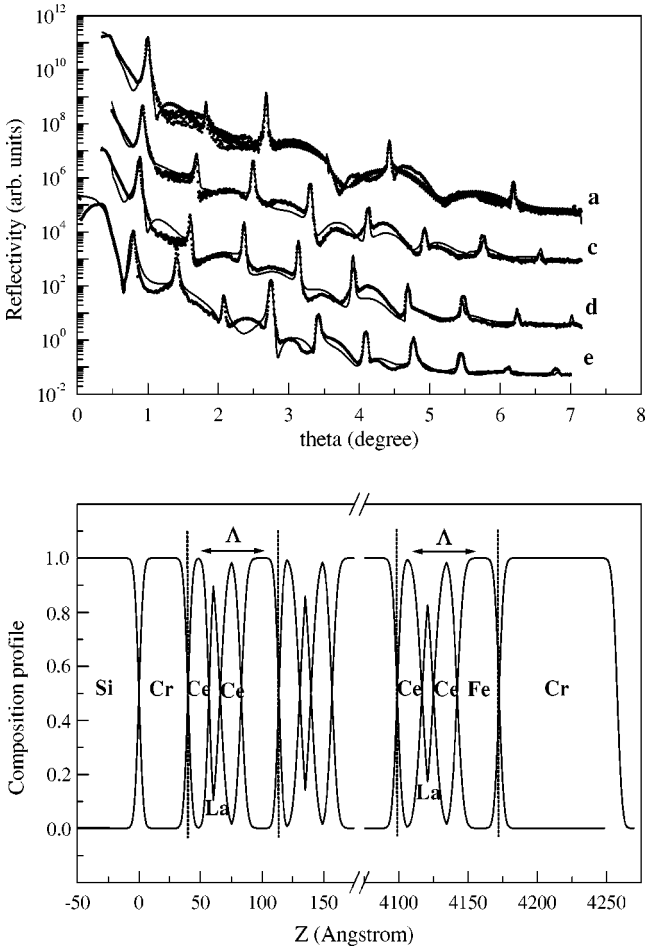

FIG. 2. Low-angle diffraction patterns from the [Ce/La/Ce/Fe] multilayers measured at 5475, 5887, 6160, and 7107 eV from top to bottom. Solid circles show the experimental results and the solid lines display the best simulations obtained for the parameters given in Table I. The inset shows the corresponding composition profile of the multilayer determined from the analysis.

TABLE I. Structural parameters for the CeLaCe/Fe multilayer. The interplanar distances correspond to (111) β fcc La, (110) bcc Fe, and (111) α Ce.

Period (Å) 73.8(0.05)	Ce	La	Ce	Fe
Layer thickness (Å)	17.1(0.8)	9.1(1)	17.1(0.8)	30.5(0.5)
Atomic density (10^{-3} Å^{-3})	35.1	26.45	35.1	84.92
Roughness (Å)	Fe/Ce	Ce/La	La/Ce	Ce/Fe
	2(0.7)	3(0.5)	3.1(0.5)	2.6(0.8)
Interplanar distance (Å)	2.85	3.03	2.85	2.027
Nb of effective pure atomic planes	6	3	6	15.05

netic profile in a sample where the introduction of hydrogen into the Ce layers implies a strain relaxation which leads to a 4*f* relocalization. In [$CeH_{2-\delta}$/Fe] multilayers, Ce is observed to adopt a γ-like electronic configuration.[19] Hence, the investigation of the Ce 5*d* magnetization for both the α and γ configurations, will allow us to discuss the influence of the 4*f* electrons on the interaction between the rare-earth (RE) and transition metal (TM).

This paper is organized as follows. In Sec. II, the sample preparation and structural characterization are described. Section III gives a brief overview of the XRMS method and presents the experimental results and magnetic profiles derived from their analysis. The sensitivity of the method for the determination of the magnetic profile is also discussed in that section. Finally Sec. IV discusses the magnetic behavior of Ce on both sides of the phase transition from the itinerant α-like to the localized γ-like phase.

II. SAMPLES CHARACTERIZATION

A. Experimental method

1. Sample preparation

Two types of multilayer systems, nominally [Fe 30 Å/Ce(La) 15 Å/La(Ce) 10 Å/Ce(La) 15 Å]$\times$57 and [Fe 30 Å/$CeH_{2-\delta}$20 Å]$\times$38 ($\delta\sim0.4$), were grown by ion-beam sputtering with argon in an ultrahigh-vacuum chamber (base pressure $<5\times10^{-10}$ mbar). Typical growth rates were near 1.0 Å/s for La and pure Ce, 0.5 Å/s for Fe, and 0.3 Å/s for the $CeH_{2-\delta}$ layer. For the first system, the sample holder was cooled to about 90 K by liquid nitrogen to minimize diffusion. For the growth of the hydride multilayer, hydrogen was introduced in the preparation chamber to a partial pressure of 8×10^{-6} mbar. Deposition was performed at room temperature. Prior to the deposition of the multilayers, a 40-Å Cr layer was deposited onto the Si(100) wafer substrate as a buffer layer. A 100-Å Cr capping layer provided protection against oxidation. Details of the procedure of the preparation have been given elsewhere.[19,20]

2. Resonant x-ray reflectivity

X-ray reflectivity experiments are commonly used to determine useful structural information such as layer thickness, effective electron density, and interfacial roughness (rms). However, conventional x-ray reflectivity is limited when it is necessary to separate out structural parameters for two layers of neighboring chemical species in the Mendeleiev table. One way to enhance the chemical contrast is to take advantage of the tunability of the incident photon energy, provided by synchrotron radiation sources. Close to an absorption edge of a chemical species the scattering factor may be resonantly modified. In this study, we use the resonant effect to change the respective scattering cross section of the different atoms present in the systems, in particular to enhance the sensitivity to the structural features of the Ce and La layers. Moreover, high-angle x-ray diffraction has been used to determine interlayer spacing and preferential orientation.

Figure 1 shows the real and imaginary parts of the energy-dependent correction terms to the atomic scattering factor for the three species to be considered. The dashed lines correspond to theoretical curves derived from Ref. 21 which do not take into account solid-state effects. Since the energy-dependent measurements have been performed in the vicinity of edges, it is required to determine precisely the experimental anomalous scattering factors. It has been done for the Ce L_2 and La L_2 edges as well as for the Fe *K* edge. The imaginary parts f'', shown as solid lines, are obtained from the measurement of the absorption coefficient by applying the

TABLE II. Structural parameters for the LaCeLa/Fe multilayer. The interplanar distances correspond to (111) β fcc La, (110) bcc Fe, and (111) α Ce.

Period (Å) 78.7(0.05)	La	Ce	La	Fe
Layer thickness (Å)	18.5(0.8)	10.7(0.8)	18.5(0.8)	31(0.5)
Atomic density (10^{-3} Å^{-3})	26.45	35.1	26.45	84.92
Roughness (Å)	Fe/La	La/Ce	Ce/La	La/Fe
	3(0.4)	2.5(0.9)	2.5(0.9)	3.3(0.4)
Interplanar distance (Å)	3.05	2.85	3.05	2.027
Nb of effective pure atomic planes	6.1	3.8	6.1	15.3

optical theorem. The real parts f' are derived from f'' by using the Kramers Kronig relationship.

The resonant x-ray reflectivity measurements were performed at room temperature at several incident photon energies in the vicinity of the $L_{2,3}$ absorption edges of Ce and La as well as in the vicinity of the Fe K edge. The measurements were carried out at ESRF on the seven-circle diffractometer installed on the French CRG-D2AM beamline.[22] The labels $a-f$, in Fig. 1 indicate the energies selected for our measurements. The spectra, measured at these different x-ray energies, exhibit strong energy-dependent effects as illustrated in Fig. 2. These effects may induce significant changes in the relative intensities of the diffraction peaks, such as the strong reduction of odd Bragg peaks as shown in the reflectivity measured at 5475 eV.

Two of our samples consist in a more complex stacking than the usual A/B one for which refinement procedures have been developed. In the course of this investigation, we adapted the SUPREX package[23] in order to simultaneously refine the reflectivity curves for a stacking composed by four layers by period.

B. Composition profile in [Fe/Ce/La/Ce] and [Fe/La/Ce/La]

Figures 2 and 3 display the specular x-ray resonant reflectivity measurements for the [Fe/Ce/La/Ce] and [Fe/La/Ce/La] multilayers, respectively. It can be noticed, from the high number (up to 10) of low-angle Bragg peaks, that the samples present a well-defined periodic stacking. The solid lines passing through the reflectivity data are the best fit obtained following the approach mentioned in the previous paragraph. In order to reduce the large number of free parameters in the refinement procedure, related to such a layered system (up to 19 parameters including the 4 layers in the multilayer period, the capping, base, and substrate layers), we assumed that the layer densities are equal to the bulk ones[4] and that the thickness of the two RE layers in direct contact with Fe are identical. This leads to 12 parameters to be determined. The insets in Figs. 2 and 3 show the composition profile of the model corresponding to the best calculations. The related parameters are given in Tables I and II. Even though the fit of the individual curves is not perfect, the intensity changes from peak to peak have been satisfactorily reproduced. This is essential since the XRMS data were recorded on top of Bragg peaks and not in between (see Sec. III A and Ref. 5). We believe that the disagreement between the experimental data and fit, occurring in the vicinity of the total reflectivity tail and in between Bragg peaks, is probably due to some oxidation of the capping layer which has not been taken into account.

The structure of the individual layers was deduced from x-ray diffraction at large angles. The 30-Å thin Fe sublayers grow in the bcc structure. Up to layer thickness of about 15 Å for La and 40 Å for Ce, the rare earths grow in the amorphous structure.[19] Nevertheless, below this critical value, x-ray absorption spectroscopy (XAS) measurements show a double peak at the Ce edge, which can be related to the α phase of Ce.[19] This suggests that, in both multilayers, Ce is strained and adopts an α-like structure.

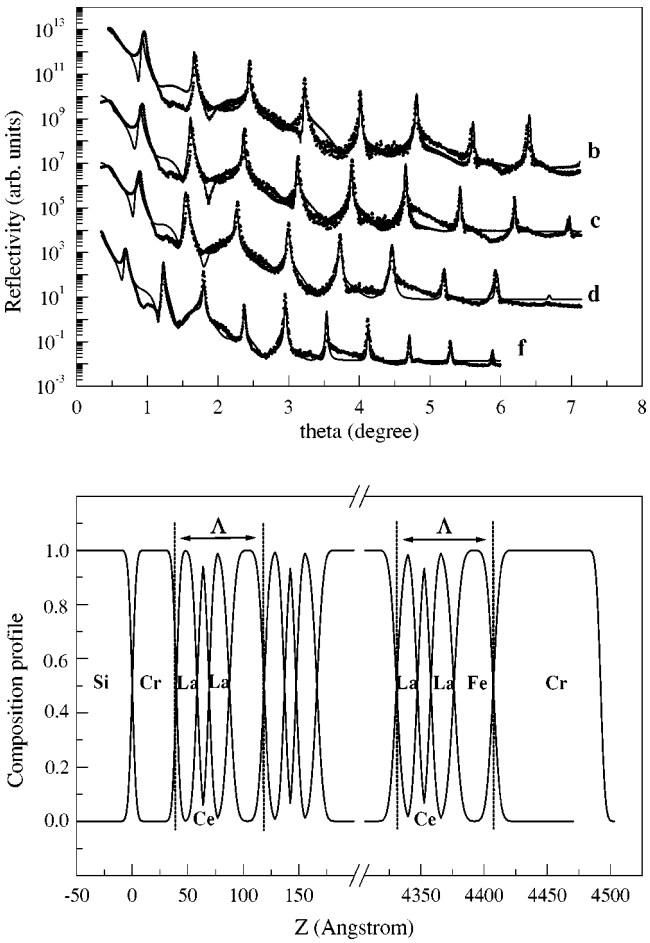

FIG. 3. Low-angle diffraction patterns from the [La/Ce/La/Fe] multilayers measured at 5715, 5887, 6160, and 7705 eV from top to bottom. Solid circles show the experimental results and the solid lines display the best simulations obtained for the parameters given in Table II. The inset shows the corresponding composition profile of the multilayer determined from the analysis.

C. Composition profile in [$CeH_{2-\delta}$/Fe]

For the hydride sample, x-ray reflectivity curves were collected at two photon energy and are displayed in the upper part of Fig. 4. The measurement at 8051 eV (Cu $K\alpha$) was carried out on a conventional setup. The data at 6200 eV, above the Ce L_2 edge, were recorded during the XRMS experiments performed at the BL39XU beamline at Spring 8. The chemical modulation of the multilayer, the thicknesses of the Fe and CeH_2 layers, as well as their interface roughness, have been refined and are given in Table III. With the assumption of densities identical to the bulk ones, nine free parameters are left in the refinement procedure. The corresponding model is shown in the lower part of Fig. 4. The simulation reproduces quite nicely the experimental data, indicating a high-quality stacking. It is worth noting that the asymmetry between the two interfacial roughness was a key parameter to satisfactorily describe the reflectivity, especially the intensity of the second-order Bragg peak.

The high-angle spectrum, displayed in the central part of Fig. 4, shows the good crystallinity of both multilayer components: Fe grows in its bcc structure and hydride Ce in a

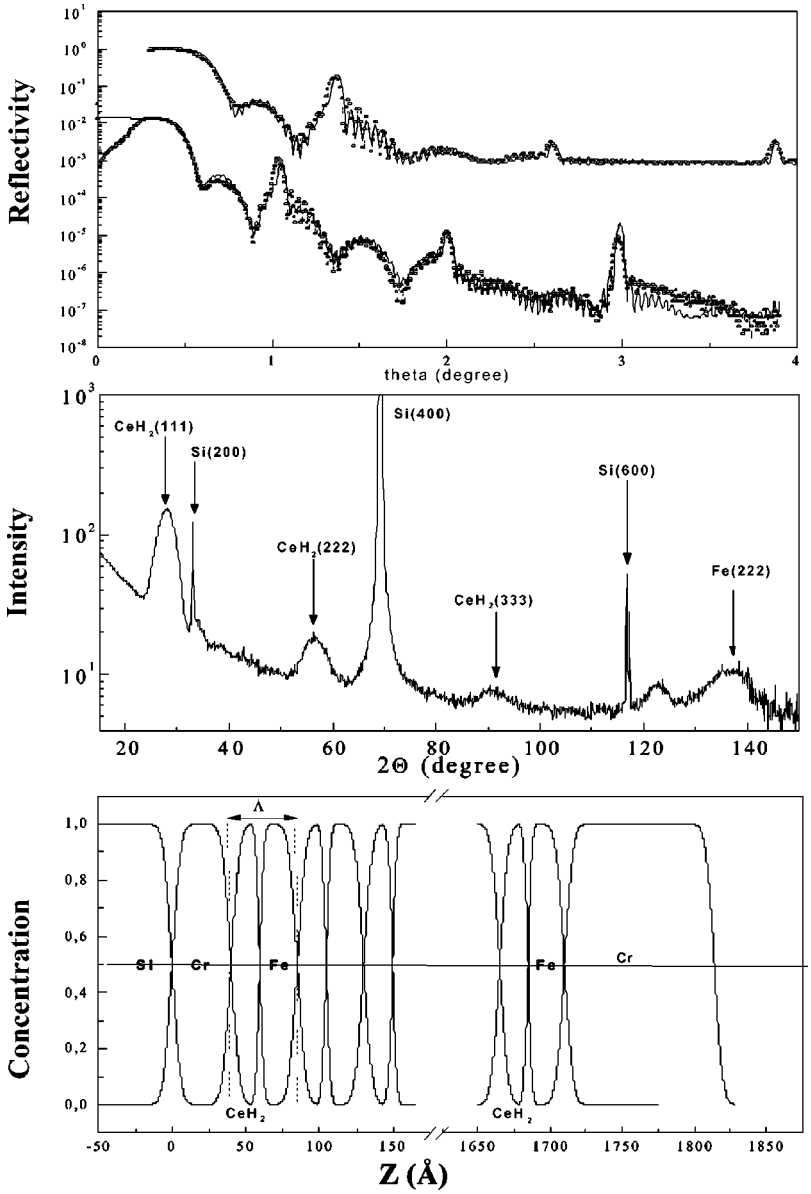

FIG. 4. Top: low-angle diffraction patterns from the $[CeH_2/Fe]$ multilayers measured at 6200 eV and 8051 eV (Cu $K\alpha$) from top to bottom. Solid circles show the experimental results and the solid lines display the best simulations obtained for the parameters given in Table III. Center: x-ray diffractograms (Cu $K\alpha$) at high scattering angles of the $[CeH_2/Fe]$ multilayers. Bottom: the composition profile of the $[CeH_2/Fe]$ multilayer determined from the analysis.

CaF_2-like fcc structure. This quality is probably due to the decrease of the lattice mismatch (from $\sim$15% to 3%), with respect to the nonhydride sample. In fact, the introduction of hydrogen reduces the strain effect in the thin film by increasing the lattice parameter, up to $a=5.57$ Å for CeH_2. Moreover, from XAS measurements previously performed,[20] which show a single white line, at the Ce L_2 edge, it has been concluded that the introduction of hydrogen reduces the strength of the 4*f*-5*d* valence-band hybridization, which leads to a relocalization of the 4*f* states.

TABLE III. Structural parameters for the CeH_2/Fe multilayer. The interplanar distances correspond to the (111) bcc Fe and the (111) γ Ce.

Period (Å) 44.95(0.05)	CeH_2	Fe
Layer thickness (Å)	19.6(0.3)	25.4(0.3)
Atomic density (10^{-3} Å^{-3})	29.1	84.92
Roughness (Å)	Fe/CeH_2	CeH_2/Fe
	3.3(0.2)	1.6(0.2)
Interplanar distance (Å)	3.2	1.7
Nb of atomic planes	6.1	15.1

III. DETERMINATION OF THE Ce MAGNETIC PROFILE

A. X-ray resonant magnetic scattering

1. Analysis method

The method is fully described in a previous paper.[4] Here, we would like to recall the main steps.

In a magnetic material, the atomic scattering factor may be written as follows:[24]

$$f=-(\hat{e}_f\cdot\hat{e}_i)[f_0+f'(E)-if''(E)]+f_{magn}^{res}.$$

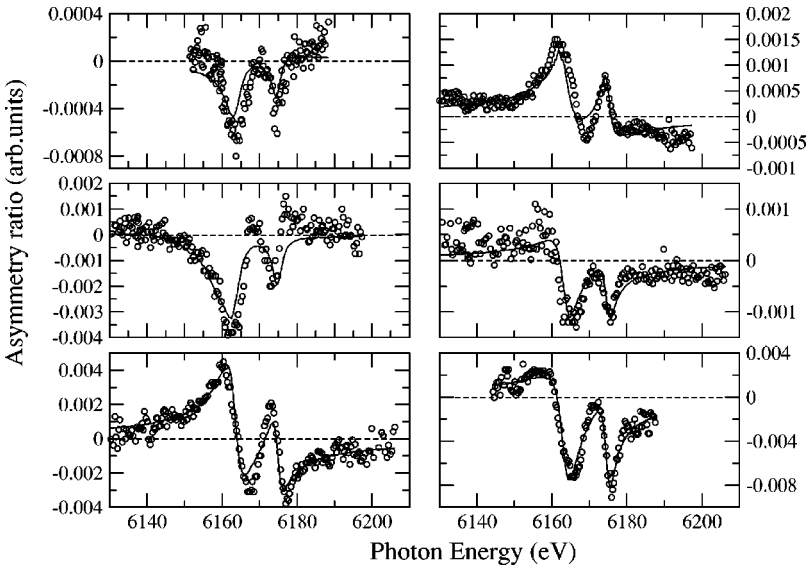

FIG. 5. Energy dependence of the asymmetry ratio at the Ce L_2 edge for six low-angle diffraction peaks of the CeLaCe/Fe multilayer. Open circles show experimental values and solid lines the simulations obtained using the profile of magnetic polarization shown in the lower part of Fig. 8.

Here f_0 is the regular charge scattering factor, and f' and f'' are the energy-dependent resonant contributions associated to an absorption edge. $\hat{e}_i$ and $\hat{e}_f$ are the polarization vectors of the electric field for the incident and scattered x-ray beams. In this investigation, the magnetic contribution to the scattering process was measured at the Ce L_2 edge because the XMCD amplitude is as high as the one at the L_3 edge and the transition ($2p^{1/2} \rightarrow 5d^{3/2}$) is purely of dipolar origin. Therefore, in the magnetization-dependent term f_{magn}^{res}, the quadrupolar contribution was neglected:

$$f_{magn}^{res} = -i(\hat{e}_f \times \hat{e}_i).\hat{z}[m'(E) - im''(E)].$$

Here $\hat{z}$ is the magnetization unit vector and m'' is equivalent to the XMCD signal.[7] In order to perform a quantitative analysis, the energy dependence of the imaginary part of the magnetic resonant scattering amplitude, m'', at the Ce L_2 edge is deduced from previous XMCD measurements[19,20] performed on similar samples. m' is derived from m'' by using the Kramers-Kronig relationship.

We now recall the refinement procedure allowing us to obtain the element-specific magnetic profile. The basis of this procedure is to calculate the energy dependence of the asymmetry ratio $R=(I^+ - I^-)/(I^+ + I^-)$, where I^+ and I^- are the diffracted intensities for the two opposite directions of the field measured at the top of several Bragg peaks. The measurements of the intensity at those positions in the reciprocal space, which originates from the interference process between periodically stacked layers, allow us to strongly reduce the influence of the the capping layer, the buffer layer, and substrate ones. As discussed in Ref. 4, the calculation can be carried out in the first Born approximation by considering a perfect multilayer. Let us define F and M as the complex charge and magnetic structure factors, respectively, q being the scattering vector and E, the energy of the incident photons. In the case of the longitudinal geometry,[4] the asymmetry ratio can be written as

$$R = \frac{-2\tau_c \cos^3(\theta)[F_r M_r - F_i M_i]}{\cos^2(\theta)|M^2| + \left(1 - \frac{K\tau_c \sin^2(2\theta)}{2}|F^2|\right)},$$

where

$$F(q,E) = F_r - iF_i = \sum_j C_j \cdot \sigma_j \cdot (f_0 + f' - if'')e^{iqr},$$

$$M(q,E) = M_r - iM_i = \sum_j \alpha_j \cdot C_j \cdot \sigma_j \cdot (m' - im'')e^{iqr}.$$

Here θ is the angle between the direction of the incident photons and the sample surface. K is the ratio of the amplitudes of the σ (vertical) and π (horizontal) components of the elliptical electric field, and the rate of circular polarization is given by $\tau_c = 2K/(1+K^2)$. In the description of the complex structure factor r is the coordinate of the atomic planes along the growth axis of the multilayer and σ_j corresponds to the planar atomic density of the layers.

In order to describe the interfacial intermixing created during the growth process, each layer is divided into slices whose composition, especially in the interfacial region, may be altered by changing the atomic concentration C_j of the different atomic species. In this study, the thickness of each slices has been defined as the wieghted sum of the thickness of the atomic layer (AL) of each type of element in the slices. The thickness of an AL corresponds to the interplanar distance deduced from the hard-x-ray measurements (Tables I, II, and III). The number and position of AL's inside the different layers constituting the chemical period, as well as the σ_j's, which are equal to the three-dimensional atomic density divided by the thickness of the individual atomic layer, and the C_j's are derived from the composition profile shown in Figs. 3–5. Therefore, the only unknown parameters are the values of the magnetic polarization for each AL. Assuming that the mean value of the magnetization over one-

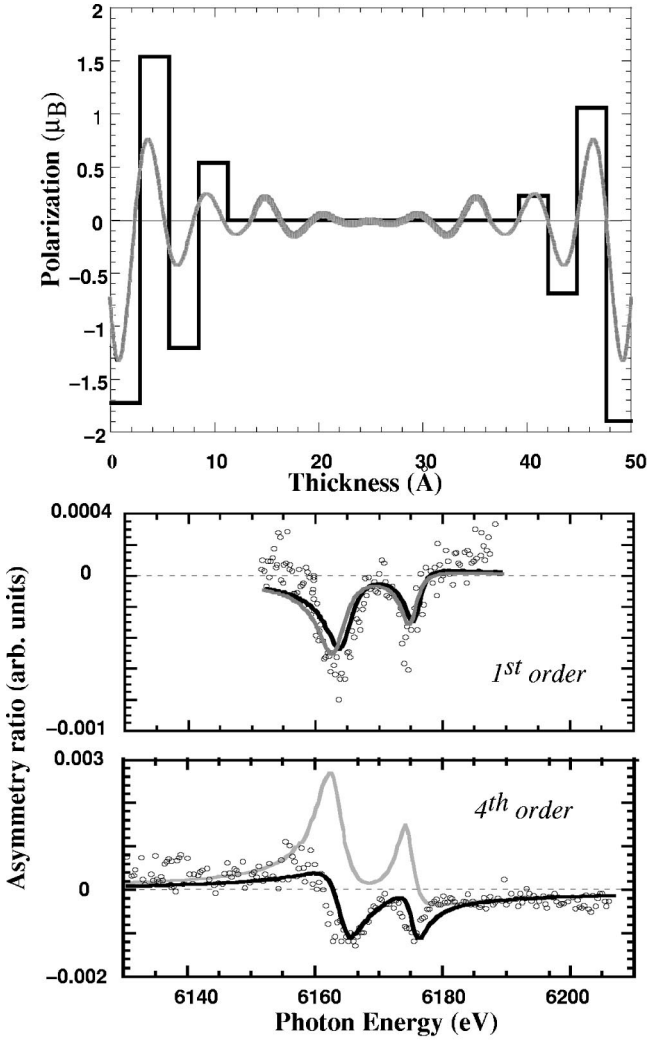

FIG. 6. Top: profile (gray) across the Ce sublayer in CeLaCe/Fe with reduced moment close to the interfaces (see text) and in black the best profile shown in the lower part of Fig. 8. Energy dependence of the asymmetry ratio for the first (center) and the fourth (bottom) low-angle Bragg peak. Gray line shows the simulation obtained using the profile displayed as solid line. Black line: the best simulation display in Fig. 5.

period is given by the XMCD amplitude, the magnetic polarization can be described as the product between the average amplitude m'-im'' and the factor α_j, called the atomic layer polarization. α_j can vary in amplitude and sign from slice to slice through the unit cell. Thus, the average of the α_j factors over the unit cell, weighted by the Ce concentration, must be equal to 1. Hence, the link between α_j parameters and the atomic magnetization in units of Bohr magnetons for one slice can easily be evaluated by multiplying α_j by the XMCD value given in μ_B, provided that value has been carefully evaluated.

The above analytical expression of the asymmetry ratio allows one to simultaneously refine the energy dependence of all R in order to determine the α_j factors in the unit cell (chemical modulation) leading to the magnetic profile inside the Ce layers.

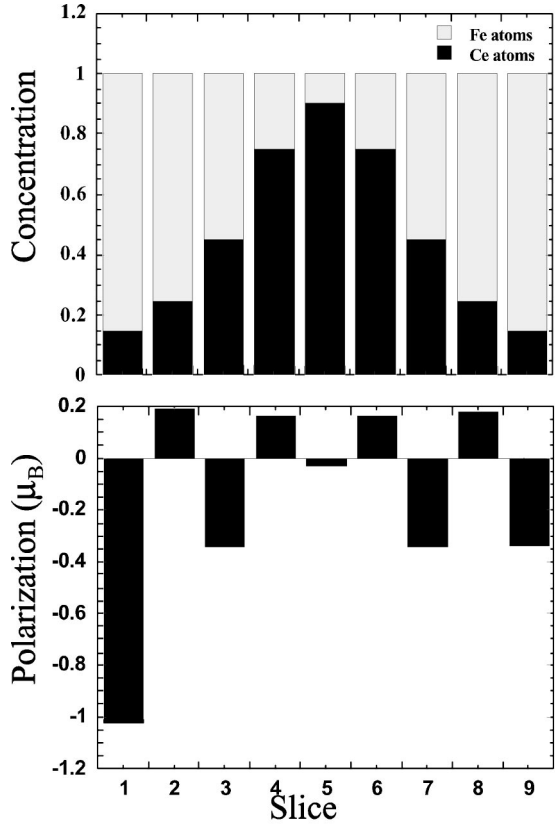

FIG. 7. Profile across the Ce sublayer in the LaCeLa/Fe multilayer, of the Ce atomic concentration, upper part, and of the Ce 5*d* induced polarization, lower part. The negative sign is taken with respect to the Fe magnetization.

2. Experimental details

The XRMS measurements on the [Fe/Ce(La)/La(Ce)/Ce(La)] multilayers were carried out at the European Synchrotron Radiation Facility (E.S.R.F.) at Grenoble on the helical undulator beamline ID12A.[25] The Daresbury two-circle diffractometer vacuum chamber[26] was set on the beamline for the experiment. The incident photons were circularly polarized with a rate of 84% at the Ce L_2 edge. A LMOKE (longitudinal magneto-optic Kerr effect) type geometry was used with the magnetic field applied in the diffraction plane and parallel to the sample surface. Energy-dependent reflectivity curves were recorded at a fixed scattering vector position, corresponding to the position of the low-angle Bragg peaks. At each data point, the saturating magnetic field was reversed to collect the reflected intensities I^+ and I^-. The magnetic asymmetry is weak as exhibited through the energy dependence of the asymmetry ratios R (Figs. 5, 6, and 9). The highly efficient detection system, as well as an excellent stability in the beam position, allows us to measure the asymmetry up to the sixth-order Bragg peak of the multilayers (Figs. 5 and 9), with a very good signal-to-noise ratio.

The XRMS measurements on the hydride $CeH_{2-\delta}$/Fe multilayer were performed at the x-ray undulator BL39XU beamline[27] at Spring-8 storage ring. During this experiment a sample holder including a permanent magnet was used. The XRMS signals were measured by using the helicity modulation technique[27] which allows us to quickly and efficiently

TABLE IV. Profiles of the values of the Ce partial density and of the 5*d* magnetic polarization across the two Ce layers in the CeLaCe/Fe sample. The unit of polarization is given in μ_B and the average over the Ce layers gives the XMCD measurement for the sample. The unit of density is that of the crystalline α phase of Ce.

Slice	1	2	3	4	5	6	7	8	9
Ce atomic concentration	0.3	0.7	1	1	1	0.8	0.55	0.2	0
Ce atomic polarization (μ_B)	−1.72	1.54	−1.2	0.54	0	0	0	0	0
Slice	10	11	12	13	14	15	16	17	18
Ce atomic concentration	0.2	0.55	0.8	1	1	1	0.8	0.6	0.4
Ce atomic polarization (μ_B)	0	0	0	0	0	0.23	−0.69	1.06	−1.89

switch the helicity of the incoming photons by flipping an x-ray diffractive phase retarder. It thus allows us to record the energy dependence of the asymmetry ratio measured on top of the four first low-angle Bragg peaks. We point out that the reversal of the applied magnetic field by rotating the sample-magnet assembly by π induced an ''opposite sign'' for the asymmetry but no change in its shape and amplitude.

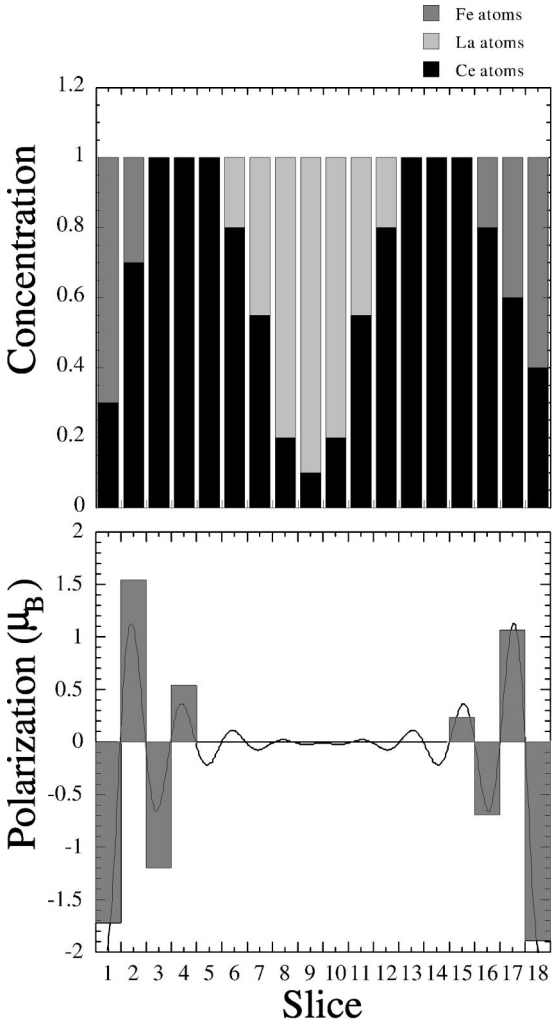

FIG. 8. Profile across the Ce sublayer in the CeLaCe/Fe multilayer, of the Ce atomic concentration, upper part, and of the Ce 5*d* induced polarization, lower part.

B. Ce 5*d* induced magnetic profile in α-like phase

Figures 5 and 9 show the energy dependence of the asymmetry ratios *R* collected at the top of chemical modulation Bragg peaks for the [Fe/Ce/La/Ce] and [Fe/La/Ce/La] multilayers. The spectral shapes exhibit a mixed behavior between pure XMCD, such as, for example, the first order displayed in Fig. 5, and a dispersionlike behavior,[28] such as, for example, the fifth order in Fig. 5. Two contributions, separated by about 10 eV, are observed and are a signature of the α-like phase of Ce. The amplitudes of *R* are rather weak, with maximum values in the range of 10^{-3}.

The first step in the analysis, as discussed in Sec. III A 1, is to define an AL by AL structural model for the unit cell. The different sublayers in the cell are centered around the La and Ce layers in the case of the [Fe/Ce/La/Ce] and [Fe/La/Ce/La] multilayers, respectively. They are divided into several slices whose thickness correspond to bulk interplanar distances: d_{111} for the β La phase, d_{111} for the α Ce, and d_{110} for bcc Fe. As mentioned in Sec. II C, the two identical RE layers are assumed to have the same thickness. In the case of the [Fe/Ce/La/Ce] multilayer, the total number of AL amounts to 15, 3, and 6 atomic layers for Fe, La, and Ce sublayers, respectively (see Table I). In order to take into account interdiffusion at interfaces, the actual number of layers, containing one kind of atom, is adjusted by using several alloy layers, the concentration of which is determined from an error function with standard deviation corresponding to the interfacial roughness derived from x-ray reflectivity (Table IV). This allow us to build the structural model displayed in the upper part of Fig. 8. The same approach was used to determine the structural model of the [Fe/La/Ce/La] multilayer (Fig. 7). For the first multilayer, it leads to a dissymmetry between the two Ce/Fe interfaces, extending over two or three AL's.

In order to derive the magnetic profile through the determination of the atomic layer magnetic polarization, it is required to reduce the numbers of free parameters which are initially equal to 18 (9 Ce containing AL's for each Ce layer) in the case of the [Fe/Ce/La/Ce] multilayer, far exceeding the number of experimental curves. This number is reduced to 17 by using the constraint that the imaginary part of the mean value of the magnetic polarization averaged over the Ce layer is given by the XMCD intensity. Second, we restricted the extension of the polarization to the 4 first planes, either mixed with Fe or pure. This assumption leads to an

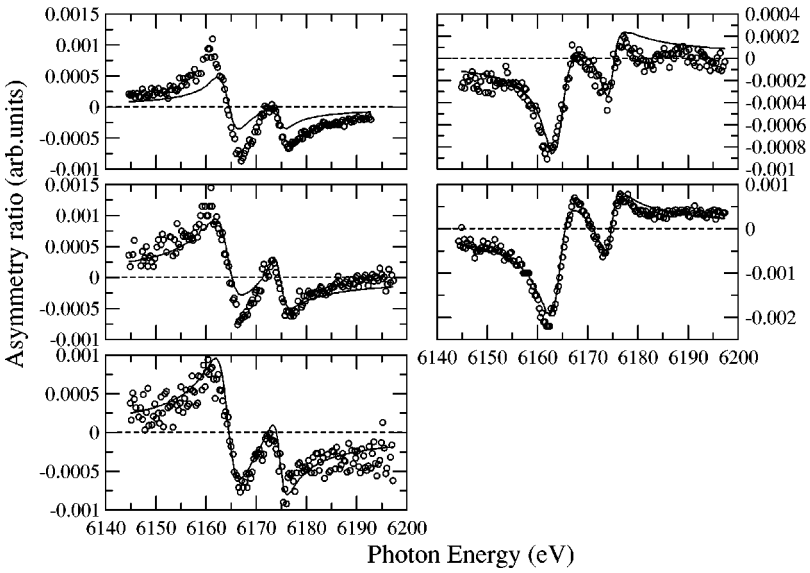

FIG. 9. Energy dependences of the asymmetry ratio at the Ce L_2 edge for six low-angle diffraction peaks of the LaCeLa/Fe multilayer. Open circles show the experimental values and solid lines the simulations obtained using the profile of the magnetic polarization shown in the lower part of Fig. 7.

extension of about 1.4 Å from the interface. This value is in close agreement with the XMCD results, obtained on several samples with different Ce thickness,[17] where the induced polarization has been found spreading out over 10–12 Å from the Fe interface. Figure 5 shows the result of the fitting procedure of the asymmetry ratios. The amplitude and the shape of the energy dependence of the asymmetry ratios measured from one low-angle Bragg peak to an other are well reproduced. The corresponding magnetic profile is displayed in the lower part of Fig. 8. This magnetic profile oscillates with a two-AL frequency and an amplitude decreasing from the Fe interfaces throughout the center of the Ce layer. The solid line displayed in the lower part of Fig. 8, which can be seen as a guide for the eyes, suggests obviously that a magnetic order may exist beyond 12 Å from the Fe interface. For this reason, it has been check that the introduction of low magnetic amplitudes beyond 12 Å into the calculation does not produce a significant change in the calculated XRMS pattern. In that sense, the simplifying assumption, which is to consider as magnetically nonpolarized all the Ce atoms beyond 11.4 Å from interface, seems to be fully suitable. We point out that models assuming a uniform magnetization throughout the Ce layer or a magnetization decreasing from the interfaces did not permit us to reproduce the experimental data. In the immediate interface, the amplitude of the magnetic moment are much higher ($-1.89\ \mu_B$) than usually observed in crystalline $CeFe_2$,[19] where magnetic moment are in the order of $-0.3\ \mu_B$. Moreover, our result does not evidence a linear relationship between magnetic moment amplitude and concentration. This is, however, in line with results in the literature which also show discrepancies for the magnetic moment for samples with the same concentration. For instance, for the well-studied $CeFe_2$ alloy, the 5*d* spin moment is measured from $-0.35\ \mu_B$ (Ref. 29) to $-0.1\ \mu_B$ (Ref. 30) by XMCD or $-0.63\ \mu_B$ (Ref. 31) by Compton scattering, whereas polarized neutrons find the corresponding moment to be only about a fifth as large: $-0.1\ \mu_B$ (Ref. 32). One explanation for the disagreement between the concentration change and magnetic amplitude change could lie on mistakes in the absolute concentration value used to describe the magnetic profile. The fact that the amplitude of the magnetization seems to be overestimated may be related to the description of the magnetic profile over only four atomic planes (limitation of the number of free parameter). Nevertheless, we emphasize that a reduction of this value, for the Ce AL close to the interface, by more than 30% leads to a huge difference between the calculated and experimental *R* values. Indeed, starting from the refined profile and reducing the moment at interface by 30%, the XRMS calculation leads to a sign reversal of *R* at the fourth multilayer Bragg peak as shown in Fig. 6. This calculation is based on a redistribution of the residual moment to the central planes to keep the average value of the moment equal to the one measured by XMCD on a similar sample. It is worth noting that the calculated *R* for the first diffraction order is unchanged whatever magnetic profile we used. It turns out to be mainly sensitive to an average view of the magnetic distribution give an information similar to XMCD. On the other hand, the more is analyzed *R* on the higher-order Bragg peak, the more is gained in spatial resolution.

For the [Fe/La/Ce/La] multilayer, the initial number of free parameters is equal to 9 (Table V). Assuming an average polarization equal to the one derived from XMCD measurements as well as a magnetic profile symmetric on both sides of the Ce layer this number is reduced to 4. This is lower than the number of five independent experimental asymmetry ratios. In order to succeed in refining simultaneously the data, the symmetrical constraint has been relaxed for the two slices on each side of the chemical profile. The magnetic profile derived from the best refinement of the asymmetry ratios is shown on the lower part of Fig. 7. We recover an oscillating behavior of the magnetic profile even in that case where there is no direct contact between Ce and Fe atoms. However, the amplitude of the magnetization is smaller and does not exhibit a sharp decrease. Nevertheless, an unexpected strong asymmetry in the polarization at the first AL is observed. Since the true parameter in the refinement procedure is the magnetic polarization of the AL, which corre-

TABLE V. Profiles of the values of the Ce partial density and of the 5*d* magnetic polarization across the two Ce layers in the LaCeLa/Fe sample. The unit of polarization is given in μ_B and the average over the Ce layers gives the XMCD measurement for the sample. The unit of density is that of the crystalline α phase of Ce.

Slice	1	2	3	4	5
Ce atomic concentration	0.15	0.25	0.45	0.75	0.9
Ce atomic polarization (μ_B)	−1.019	0.195	−0.342	0.163	−0.035
(error bars)	(0.06)	(0.05)	(0.03)	(0.04)	(0.025)
Slice	6	7	8	9	
Ce atomic concentration	0.75	0.45	0.25	0.15	
Ce atomic polarization (μ_B)	0.163	−0.342	0.179	−0.340	
(error bars)	(0.04)	(0.02)	(0.05)	(0.05)	

sponds to the actual atomic polarization times the concentration, the origin of this unexpected difference might be ascribed to a slight chemical asymmetry between the Ce/La interfaces which was not been taken into account in the composition profile. In a similar way we observe, for the [Fe/La/Ce/La] sample, that the polarization in the central layer was not critical, leading us to keep it constant in the refinement procedure. Different refinements for a set of magnetic polarization in this central slice were performed and taken into account in the errors bars displayed in Table V.

We would like to point out that, as in the [Ce/Fe] multilayers, the magnetic profile can be discussed by means of two main characteristics: an oscillatory behavior with a period of two atomic slices and a decay of the magnetization amplitude from the interface with Fe to the center of the rare-earth layer.

C. Ce 5*d* induced magnetic profile in γ-like phase

Figure 10 displays the energy dependence of the asymmetry ratios measured at the Ce L_2 edge on top of the four first Bragg peaks of the $[CeH_{2-\delta}/Fe]$ multilayer. Because of the period ($\Lambda = 45$ Å), which is smaller than the samples previously addressed in this paper, only four peaks were accessible with a satisfactory signal-to-noise ratio for the weak measured amplitude ranging from 4×10^{-4} to 3×10^{-3}. The spectral shape exhibits a unique predominant resonance (or its derivative), which is characteristic of the γ phase of Ce, according to XMCD results.[19]

The 19.6-Å $CeH_{2-\delta}$ layer is described by 6.1 effective AL's distributed over 9 Ce-containing layers (Table VI). Each one has an individual thickness corresponding to the (111) γ-Ce interplanar distance, resulting from the high-angle x-ray diffraction measurement shown in Fig. 4. The structural model, which takes into account the asymmetry between the top and bottom interfaces (Table III), is presented in the upper part of Fig. 11. Before starting the refinement procedure, aiming at the determination of the magnetic profile through the thin $CeH_{2-\delta}$ layer, it is worth noting the sign reversal between the odd and even structural Bragg peaks. It can be related, for a system with a two-layer chemical periods, to a magnetic polarization localized at the immediate interface, as previously observed in [La/Fe] (Ref. 4) and [Fe/Gd] (Ref. 13) multilayers. This conclusion cannot be extended to more complex systems with, for example an inserted nonmagnetic layer between two magnetic ones, as shown in Fig. 9 in Sec. III B. This remark prompts us to assume that the magnetization profile is restricted close to the Fe interfaces. Hence, only the magnetization amplitude

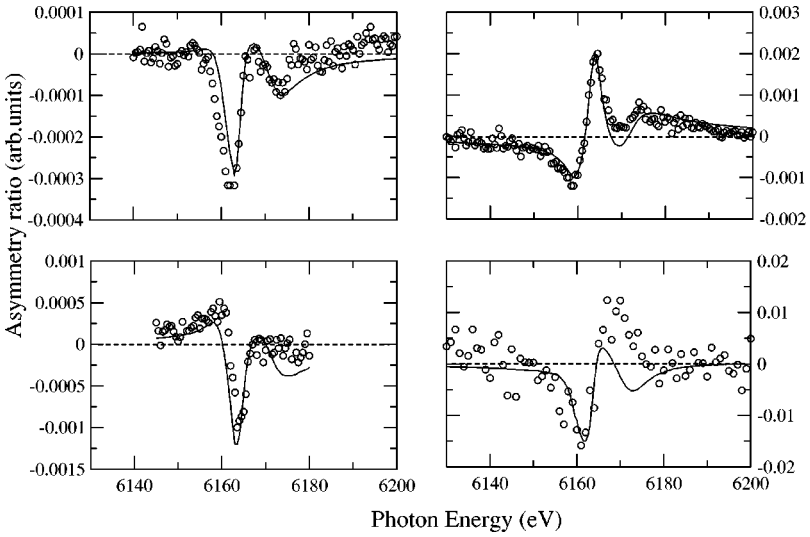

FIG. 10. Energy dependences of the asymmetry ratio at the Ce L_2 edge for four low-angle diffraction peaks of the CeH_2/Fe multilayer. Open circles show experimental values and solid lines the simulations obtained using the profile of the magnetic polarization shown in the lower part of Fig. 11.

TABLE VI. Profiles of the values of the CeH_2 partial density and of the 5*d* magnetic polarization across the two Ce layers in the CeH_2/Fe sample. The unit of polarization is given in μ_B and the average over the CeH_2 layers gives the XMCD measurement for the sample. The unit of density is that of the crystalline γ phase of Ce.

Slice	1	2	3	4	5
Ce atomic concentration	0.1	0.37	0.85	1	1
Ce atomic polarization (μ_B)	−0.325	−0.10	−0.019	0	0
(error bars)	(0.08)	(0.02)			
Slice	6	7	8	9	
Ce atomic concentration	1	0.85	0.55	0.35	
Ce atomic polarization (μ_B)	0	−0.019	−0.103	−0.325	
(error bars)			(0.015)	(0.03)	

on the three intermixed planes at interfaces will be refined. This leads to six free parameters, further reduced to five, by assuming again that the amplitude of the average magnetic polarization is equivalent to that derived from XMCD measurements. The solid line in Fig. 10 represents the best fit obtained with the corresponding magnetic profile on the lower part of Fig. 11. The agreement for the fourth order is poorer, probably due to the lower signal-to-noise ratio. Nevertheless, this fourth order is crucial in the refinement procedure as discussed in the following section. We point out that refinement procedures with different starting profiles such as constant or oscillatory, as observed in free hydrogen [Ce/Fe] multilayers, have been carried out. It always ends up with a sharply continuously decreasing magnetic profile, the comparison between all of them give the errors bars contained in Table VI.

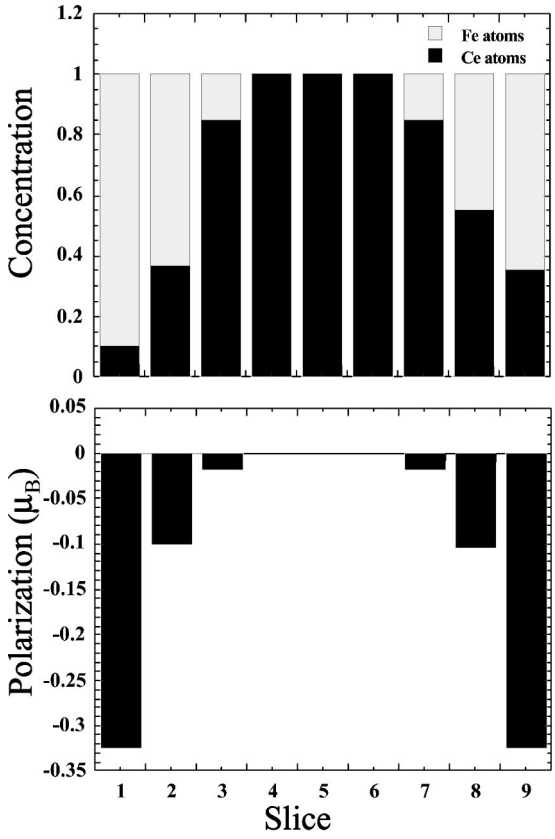

FIG. 11. Profiles of the Ce concentration (upper part) and the Ce 5*d* polarization (lower part) across the Ce sublayer in the CeH_2/Fe multilayer.

D. Sensitivity of the approach

In this section, we would like to emphasize both the advantages and limitations of the approach employed to investigate the magnetic profile in magnetic multilayers. The main advantage lies in the fact that XRMS allows one to probe q_z and hence directly provides information on the arrangement of the magnetic moments throughout thin buried layers along the stacking direction. To illustrate the sensitivity of the method, we perform a calculation for different 5*d* magnetic profile induced in the $CeH_{2-\delta}$ sublayers in the $[CeH_{2-\delta}/Fe]$ multilayer, keeping constant the magnetization average over the $CeH_{2-\delta}$ layer. Figure 12 shows the energy-dependent asymmetry ratio for a constant (left side) and an oscillating magnetic profile (right side), calculated by using the same structural model. We observe a clear difference between the calculated and experimental curves for the constant profile. In the case of an oscillatory profile, the comparison is almost satisfactory for the first, second, and third Bragg peaks with the exception of the amplitude at the maximum of the asymmetry. However, the asymmetry ratio of the fourth peak rules out that model. This clearly demonstrates the potentiality of this approach to describe the magnetic distribution. We point out that we observe the same high sensitivity for the two other multilayers studied in this work. An alternative method to investigate the depth profile of the magnetization is to analyze the change in the XMCD amplitude measured for a series of samples with different thicknesses of the magnetic layer.[33,34] One difficulty of this approach is that the structural properties of each sample may be different. Indeed, the roughness or intermixing, the homogeneity of the strain, for example, may depend on the layer thickness[35] and number of repetitions.[36] Therefore, since the magnetic properties of thin films are sensitive to the structural parameters,[37] this method may be contested. As XMCD yields average information on the magnetic properties of the layers, changes in the amplitude of magnetic moment, with regard to the thickness or to a damped antiferromagnetic order, may be misinterpreted.[4]

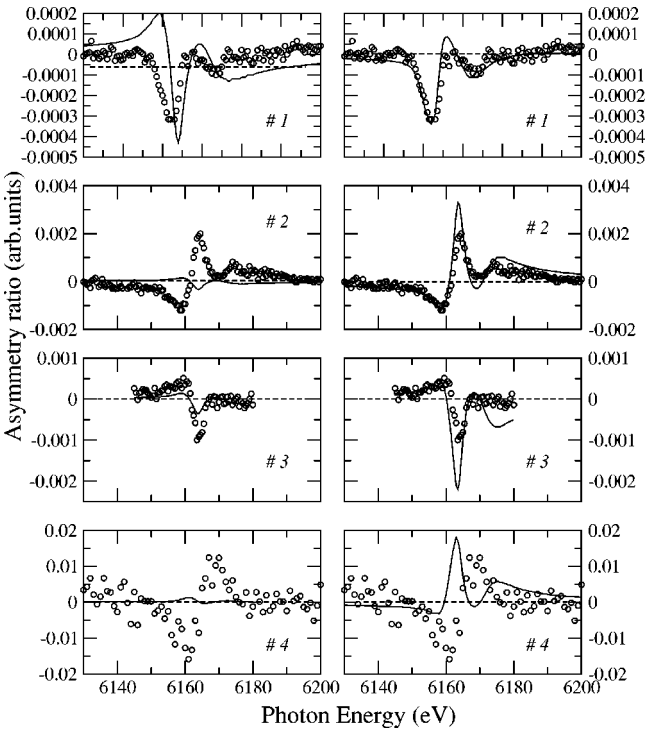

FIG. 12. Energy dependence of the asymmetry ratios at the Ce L_2 edge for four low-angle diffraction peaks of the CeH_2/Fe multilayer. Open circles show experimental values and solid lines the simulations obtained using a uniform magnetization across the CeH_2 sublayer (left part) and an oscillating model (right part).

On the contrary XRMS us allows to investigate the magnetic properties of one sample and to draw conclusions on the magnetic profile.

However, since the magnetic signal is a cross term between charge scattering and magnetic scattering (see Sec. III A), it is mandatory to obtain a precise knowledge of the structural parameters to separate out the magnetic contribution to the signal from the structural one (such as intermixing or roughness). Moreover, although XRMS allows us to obtain relevant information on the magnetic profile, it is more difficult to discuss on the absolute value of the magnetization of each atomic slice. The first reason lies in the use of XMCD data for the determination of the resonant parameters sensitive to magnetic properties which implies that XRMS is bound to the limitation of XMCD in deriving the magnetic amplitude. Another point, restricting this approach, is that the number of free parameters results from a compromise and directly relies on the ratio of the layer thickness to the distance between the atomic layers. Therefore, that number increases with layer thickness, imposing either constraints like symmetrical profiles, nonmagnetic layers, or a loss in the spatial resoluation by using slices thicker than an atomic layer. For example, in this study the number of free parameters in the refinement procedure increases from 9 for the thin $[CeH_{2-\delta}/Fe]$ multilayer to 18 for the [CeLaCe/Fe] multilayer. This implies introducing a starting hypothesis which naturally raises a question about the validity of those hypotheses such as the accuracy of the description of the interfaces (number and concentration of intermixed planes with regards to a roughness parameter) or as the assumed symmetry of the magnetic profile.

IV. DISCUSSION

The results presented above provide information on the 5*d* magnetic polarization of Ce for both the α-like and γ-like phases. An antiferromagneticlike (AF-like) ordering of α-like Ce is found in both [Ce/La/Ce/Fe] and [La/Ce/La/Fe] multilayers. They exhibit a quite different behavior concerning the amplitude of the 5*d* magnetization. For [Ce/La/Ce/Fe] the amplitude is found to continuously decrease from the Ce/Fe interface over two intermixed and two pure layers. Some of the Ce layers are found to be nonmagnetic, but this may be related to the limitation of the technique when dealing with a too large number of Ce-containing layers. The study shows the extension of the polarization from one interface into the layer. For the [La/Ce/La/Fe] sample the situation is more complex. In fact, the uniformity of the amplitude did not seem to reach from such a mechanism. Another interesting point holds in the fact that this amplitude is much more smaller than that of the first sample. A constant amplitude, when Ce atoms are not in direct contact with Fe, was also observed by XMCD (Ref. 18) by inserting a La layer of difference thickness in between the Fe and Ce sublayers. This suggest that this unexpected behavior of the Ce 5*d* polarization is an intrinsic property of α-like Ce in such strained multilayers. This argument is supported by the profile observed in the hydride sample. In fact, the introduction of hydrogen into the Ce layers leads to a vanishing of the strain as previously observed.[22] It implies a relocalization of the 4*f* electrons. Hence Ce switches to its γ-like phase and thus adopts a 5*d* magnetic profile similar to the one of La in [La/Fe] multilayers.[4] It is restricted to the interface and decreases sharply through the Ce layer. In this case our XRMS-derived profile is in agreement with the XMCD-derived one.

We like to mention recent work performed on $CeFe_2$ (Ref. 37) and doped $Ce(Fe_{1-x}Co_x)_2$ (Ref. 38) compounds with cubic laves phase structure in which the Ce 4*f* electrons are itinerant.[18] Experiment, of inelastic neutron scattering on the itinerant ferromagnet (FM) $CeFe_2$ clearly show the existence of an AF fluctuation with a wave vector $Q=[\frac{1}{2}\frac{1}{2}\frac{1}{2}]$, which modulates the Fe moments in the FM-ordered ground state.[37] This spin wave appears to have a 400-Å correlation length at low temperature which decreases with higher temperature but still exists at 300 K. The AF fluctuation was also observed by magnetic measurements depending on the doping rate in $Ce(Fe_{1-x}Co_x)_2$.[38] Unfortunately the behavior of the Ce magnetization could not be resolved in these measurements due to the small value (less than 0.04 μ_B per atom) expected from neutron scattering. The situation is not the same in the Ce-based multilayers but they give us some guidance in the understanding of the complex situation in the electronic properties of Ce compounds. Our work leads us to speculate that this AF-ordered ground state could reflect the existence of an AF ordering on the Ce 5*d* electrons similarly as described in this paper. The spin structure might be transferred to the 3*d* states of Fe in $Ce(Fe_{1-x}Co_x)_2$, in which Ce

and Fe atoms are always in direct contact, through the direct exchange coupling of the Fe 3*d* and Ce 5*d* electrons.

V. CONCLUSION

To summarize, the behavior of the magnetic polarization of the α-like Ce sublayers in the multilayers can be described by two main components. The first feature is an intrinsic AF magnetic order (amplitude $\sim 0.2\ \mu_B$) which persist even if the strained Ce layer is separate from the Fe layer by a La one. The second characteristic is an increase of the 5*d* polarization of Ce atoms intermixed with Fe. It is followed by a damped decrease while keeping the AF structure. The enhancement is probably due to a contribution of Fe the 3*d* states to the 5*d* magnetic polarization by a direct hybridization.

Moreover, we unambiguously demonstrate the key role of the 4*f* electrons whose relocalization, induced by a strain relaxation into the Ce layer, leads to the disappearance of the AF order. This must be related to the calculation of Min *et al.*[39] who show that there is a very-low-energy difference between paramagnetic, FM and AF states for Ce in its α-like phase on the borderline to the transition into the γ-like phase. Our XRMS experiment suggests that the strain inside the Ce film, via an effect on 4*f* states, could be at the origin of subtle change in the electronic configuration of α-like Ce. It might modify this energy difference and induce an AF order on the Ce 5*d* states. The experiments have also to be related to the absence of a XMCD signal at the Ce $M_{IV,V}$ edges in [LaCeLa/Fe] which could be due either to a 4*f* magnetic moment equal to zero or to a perfect AF order of the α-like Ce 4*f* states in such multilayers when there is no direct Fe/Ce interface. In that sense a similar XRMS experiment at the Ce $M_{IV,V}$ edge has been performed[40] to directly probe the magnetic state of Ce 4*f* electrons in both the *itinerant* and *localized* states. The data are now being analyzed.

Finally we think that XRMS associated with a detailed structural investigation offers a unique possibility to selectively distinguish between different magnetic arrangements in artificial magnetic structures.

[1] I.K. Schuller, Phys. Rev. Lett. **44**, 1597 (1980).
[2] B.Y. Jin and J.B. Ketterson, Adv. Phys. **38**, 189 (1989).
[3] Ivan K. Schuller, S. Kim, and C. Leighton, J. Magn. Magn. Mater. **200**, 571 (1999).
[4] L. Sève, N. Jaouen, J.M. Tonnerre, D. Raoux, F. Bartolomé, M. Arend, W. Felsch, A. Rogalev, J. Goulon, C. Gautier, and J.F. Bérar, Phys. Rev. B **60**, 9662 (1999).
[5] F. de Bergevin and M. Brunel, Phys. Lett. **39A**, 141 (1972).
[6] C.C. Kao, C.T. Chen, E.D. Johnson, J.B. Hastings, H.J. Lin, G.H. Ho, G. Meigs, J.-M. Brot, S.L. Hulbert, Y.U. Idzerda, and C. Vettier, Phys. Rev. B **50**, 9599 (1994).
[7] J.M. Tonnerre, L. Sève, D. Raoux, G. Soullié, B. Rodmacq, and P. Wolfers, Phys. Rev. Lett. **75**, 740 (1995).
[8] Y.U. Idzerda *et al.*, Synchrotron Radiat. News **10**, 6 (1997).
[9] M. Sacchi and A. Mirone, Phys. Rev. B **57**, 8408 (1998).
[10] C.C. Kao, J.B. Hastings, E.D. Johnson, D.P. Siddons, G.C. Smith, and G.A. Prinz, Phys. Rev. Lett. **65**, 373 (1990).
[11] J.M. Tonnerre, L. Sève, D. Raoux, B. Rodmacq, M. De Santis, P. Troussel, J.M. Brot, V. Chakarian, C.C. Kao, E.D. Johnson, and C.T. Chen, Nucl. Instrum. Methods Phys. Res. B **97**, 444 (1995).
[12] A. Déchelette, J.M. Tonnerre, M.C. Saint Lager, F. Bartolomé, L. Sève, D. Raoux, H. Fischer, M. Piecuch, V. Chakarian, and C.C. Kao, Phys. Rev. B **60**, 6636 (1999).
[13] N. Ishimatsu, H. Hashizume, S. Hamada, N. Hosoito, C.S. Nelson, C.T. Venkataraman, G. Srajer, and J.C. Lang, Phys. Rev. B **60**, 9596 (1999).
[14] N. Jaouen, J.M. Tonnerre, E. Bontempi, D. Raoux, L. Sève, F. Bartolomé, A. Rogalev, M. Menzenberg, W. Felsch, H.A. Dürr, E. Dudzik, and H. Maruyam, Physica B **283**, 175 (2000).
[15] L. Sève, J.M. Tonnerre, D. Raoux, J.F. Bobo, M. Piecuch, M. De Santis, P. Trouseel, J.M. Brot, V. Chakarian, C.C. Kao, and C.T. Chen, J. Magn. Magn. Mater. **148**, 68 (1995).
[16] T.P.A. Hase, I. Pape, D.E. Read, B.K. Tanner, H. Dürr, E. Dudzik, G. van der Laan, C.H. Marrows, and B.J. Hickey, Phys. Rev. B **61**, 15 331 (2000).
[17] F. Klose, O. Schulte, F. Rose, W. Felsch, S. Pizzini, C. Giorgetti, F. Baudelet, E. Dartyge, G. Krill, and A. Fontaine, Phys. Rev. B **50**, 6174 (1994).
[18] O. Eriksson, L. Nördström, M.S.S. Brooks, and B. Johansson, Phys. Rev. Lett. **60**, 2523 (1988).
[19] M. Arend, M. Finazzi, O. Schulte, M. Münzenberg, A.-M. Dias, F. Baudelet, Ch. Giorgetti, E. Dartyge, P. Schaaf, J.-P. Kappler, G. Krill, and W. Felsch, Phys. Rev. B **57**, 2174 (1998).
[20] M. Arend, W. Felsch, G. Krill, A. Delobbe, F. Baudelet, E. Dartyge, J.-P. Kappler, M. Finazzi, A. San Miguel-Fuster, S. Pizzini, and A. Fontaine, Phys. Rev. B **59**, 3707 (1999).
[21] B.L. Henke, E.M. Gullikson, and J.C. Davis, At. Data Nucl. Data Tables **54**, 181 (1993).
[22] J.L. Ferrer, J.P. Simon, J.F. Bérar, B. Caillot, E. Fanchon, O. Kaikati, S. Arnaud, M. Pirrochi, and M. Roth, J. Synchrotron Radiat. **5**, 1346 (1998).
[23] E.E. Fullerton, J. Pearson, C.H. Sowers, S.D. Bader, X.Z. Wu, and S.K. Sinha, Phys. Rev. B **48**, 17 432 (1993).
[24] J.P. Hannon, G.T. Trammell, M. Blume, and D. Gibbs, Phys. Rev. Lett. **61**, 1245 (1988); **62**, 2644(E) (1989).
[25] J. Goulon, A. Rogalev, C. Gauthier, C. Goulon-Ginet, S. Paste, R. Signorato, C. Neumann, L. Varga, and C. Marlgrange, J. Synchrotron Radiat. **5**, 232 (1998).
[26] G. Van der Laan, H.A. Dürr, E. Dudzik, M.D. Roper, S.P. Collins, T.P.A. Hase, and I. Pape, Synchrotron Radiat. News **12**, 5 (1999).
[27] M. Suzuki, N. Kawamura, M. Mizumaki, A. Urata, H. Maruyama, S. Goto, and T. Ishikawa, J. Synchrotron Radiat. **6**, 190 (1999).
[28] See Fig. 1 in Ref. 4.
[29] A. Delobbe, A.-M. Dias, M. Finazzi, L. Stichauer, J.-P. Kappler, and G. Krill, Europhys. Lett. **43**, 320 (1998).
[30] C. Giorgetti, S. Pizzini, E. Dartyge, A. Fontaine, F. Baudelet, C. Brouder, P. Bauer, G. Krill, S. Miraglia, D. Fruchart, and J.-P. Kappler, Phys. Rev. B **48**, 12 732 (1993).
[31] M.J. Cooper, P.K. Lawson, M.A.G. Dixon, E. Zukowski, D.N.

Timms, F. Itoh, H. Sakurai, H. Kawata, Y. Tanaka, and M. Ito, Phys. Rev. B **54**, 4068 (1996).
[32] S.J. Kennedy, P. Brown, and B.R. Coles, J. Phys.: Condens. Matter **5**, 5169 (1993).
[33] J. Vogel, A. Fontaine, V. Cros, F. Petroff, J.-P. Kappler, G. Krill, A. Rogalev, and J. Goulon, Phys. Rev. B **55**, 3663 (1997).
[34] F. Wilhelm, P. Poulopoulos, G. Ceballos, H. Wende, K. Baberschke, P. Srivastava, D. Benea, H. Ebert, M. Angelakeris, N.K. Flevaris, D. Niarchos, A. Rogalev, and N.B. Brookes, Phys. Rev. Lett. **85**, 413 (2000).
[35] J. Shen, P. Ohresser, Ch.V. Mohan, M. Klaua, J. Barthel, and J. Kirschner, Phys. Rev. Lett. **80**, 1980 (1998).
[36] A. Déchelette, M.C. Saint-Lager, J.M. Tonnerre, G. Patrat, D. Raoux, H. Fischer, S. Andrieu, and M. Piecuch, Phys. Rev. B **60**, 6623 (1999).
[37] L. Paolasini, P. Dervenagas, P. Vulliet, J.P. Sanchez, G.H. Lander, A. Hiess, A. Panchula, and P. Canfield, Phys. Rev. B **58**, 12 117 (1998).
[38] R.J. Lange, I.R. Fisher, P.C. Canfield, V.P. Antropov, S.J. Lee, B.N. Harmon, and D.W. Lynch, Phys. Rev. B **62**, 7084 (2000).
[39] B.I. Min, H.J.F. Jansen, T. Oguchi, and A.J. Freeman, Phys. Rev. B **34**, 369 (1986).
[40] N. Jaouen (unpublished).